VU VRIJE UNIVERSITEIT AMSTERDAM

# VU Research Portal

## Understanding the open circuit voltage in organic solar cells on the basis of a donor-acceptor abrupt (p-n++) heterojunction

Nolasco, J. C.; Castro-Carranza, A.; León, Y. A.; Briones-Jurado, C.; Gutowski, J.; Parisi, J.; von Hauff, E.

***published in***
Solar Energy
2019

***DOI (link to publisher)***
10.1016/j.solener.2019.04.031

***document version***
Publisher's PDF, also known as Version of record

***document license***
Article 25fa Dutch Copyright Act

**Link to publication in VU Research Portal**

***citation for published version (APA)***
Nolasco, J. C., Castro-Carranza, A., León, Y. A., Briones-Jurado, C., Gutowski, J., Parisi, J., & von Hauff, E. (2019). Understanding the open circuit voltage in organic solar cells on the basis of a donor-acceptor abrupt (p-n++) heterojunction. *Solar Energy*, *184*, 610-619. https://doi.org/10.1016/j.solener.2019.04.031

**General rights**
Copyright and moral rights for the publications made accessible in the public portal are retained by the authors and/or other copyright owners and it is a condition of accessing publications that users recognise and abide by the legal requirements associated with these rights.

- Users may download and print one copy of any publication from the public portal for the purpose of private study or research.
- You may not further distribute the material or use it for any profit-making activity or commercial gain
- You may freely distribute the URL identifying the publication in the public portal ?

**Take down policy**
If you believe that this document breaches copyright please contact us providing details, and we will remove access to the work immediately and investigate your claim.

**E-mail address:**
**vuresearchportal.ub@vu.nl**

Download date: 05. May. 2023

Solar Energy 184 (2019) 610–619

Contents lists available at ScienceDirect

Solar Energy

journal homepage: www.elsevier.com/locate/solener

# Understanding the open circuit voltage in organic solar cells on the basis of a donor-acceptor abrupt (p-n++) heterojunction

J.C. Nolasco[a,b,*], A. Castro-Carranza[c,d], Y.A. León[d], C. Briones-Jurado[d], J. Gutowski[c,e], J. Parisi[a], E. von Hauff[f]

[a] Energy and Semiconductor Research Laboratory, Department of Physics, Carl von Ossietzky University of Oldenburg, 26111, Germany
[b] Micro and Nanotechnology Research Centre MICRONA, Veracruz University, 94294 Veracruz, Mexico
[c] Semiconductor Optics, Institute of Solid State Physics, University of Bremen, 28359 Bremen, Germany
[d] Science of Sustainable Materials, National School of Higher Studies Unit Morelia, National Autonomous University of Mexico (ENES Morelia UNAM), 58190 Morelia, Mexico
[e] MAPEX Center of Materials and Processes, University of Bremen, 28359 Bremen, Germany
[f] Physics of Energy, Department of Physics and Astronomy, Vrije Universiteit Amsterdam, 1081 Amsterdam, the Netherlands

ARTICLE INFO

*Keywords:*
Open circuit voltage
Organic heterojunction
Band bending

ABSTRACT

By using electrical characterization and classical solid state semiconductor device theory, we demonstrate that the open circuit voltage ($V_{oc}$) in organic solar cells based on non-intentional doped semiconductors is fundamentally limited by the built-in potential ($V_{bi}$) originated at a donor-acceptor abrupt (p-n$^{++}$) heterojunction in case of selective contacts. Our analysis is validated using P3HT:PCBM devices fabricated in our research group. We also demonstrate that such a result can be generalized using data already reported in literature for fullerene-based solar cells. Finally, we show that the dependence of $V_{oc}$ on the device contacts can be understood in terms of the potential barriers formed by the Fermi level alignment of semiconductors at the heterojunction and at the Schottky junctions.

## 1. Introduction

The open circuit voltage is one of the fundamental parameters defining the efficiency of solar cells. In organic ones, losses leading to reduced $V_{oc}$ have been attributed to different regions within the device (Cheyns et al., 2008; Burke et al., 2015), such as contact surfaces (Xia et al., 2013), bulk trap states (Hawks et al., 2014; Ripolles et al., 2013; Blakesley and Neher, 2011), and the internal heterojunction interface (Burke et al., 2015; Vandewal et al., 2008, 2014, 2009; Graham et al., 2013). For devices with ohmic or selective contacts, it has been proposed that the predominant recombination processes occur at the internal donor-acceptor heterojunction interface, and that the recombination rate is correlated with $E_{D\text{-}A}$ (Perez et al., 2009; Potscavage et al., 2008), where $E_{D\text{-}A}$, given by the energy difference between the Highest Occupied Molecular Orbital of the donor ($HOMO_D$) and the Lowest Unoccupied Molecular Orbital of the acceptor ($LUMO_A$).

Extensive work has been done to relate the electronic properties of the interface to recombination phenomena. Particularly, using optical spectroscopy methods, it has been shown that recombination at the heterojunction can be reduced by increasing the molecular order in the fullerene (Veldman et al., 2008) and polymer (Hallermann et al., 2009) domains, promoting charge separation via increased carrier delocalization (Gélinas et al., 2014). Vandewal et al. (2014) demonstrated that most photoexcited carriers eventually relax to lowest emissive localized interfacial state ($E_{CT}$) and are already in quasi-thermal equilibrium before charge separation occurs. It is now clear that $V_{oc}$ losses can be quantified by considering energetic disorder (Hawks et al., 2014; Ripolles et al., 2013; Blakesley and Neher, 2011). On this basis, the electrostatics at the donor/acceptor junction arising from disorder effects in organic solar cells has been considered in studies of $V_{oc}$. Thus, by using molecular simulations, Poelking et al. (2015) showed that the structural ordering of the active layer molecules can be linked to the chemical potential or Fermi level. They applied these results to predict $V_{oc}$ in a series of organic heterojunctions. Such an analysis supported a theory with a predominant flat band situation in the non-intentionally doped cells as a general phenomenon caused by mesoscale order. However, the capacitance vs. voltage (C-V) characteristics of numerous functional systems indicates that band bending fully extends within the semiconductor with the lower charge carrier concentration (Liu et al., 2008; Guerrero et al., 2013; Dibb et al., 2013; Deledalle et al., 2015;

* Corresponding author at: Micro and Nanotechnology Research Centre MICRONA, Veracruz University, 94294 Veracruz, Mexico.
*E-mail addresses:* jairo.cesar.nolasco.montano@uni-oldenburg.de, janolasco@uv.mx (J.C. Nolasco).

https://doi.org/10.1016/j.solener.2019.04.031
Received 25 November 2018; Received in revised form 27 February 2019; Accepted 8 April 2019
Available online 13 April 2019
0038-092X/ © 2019 International Solar Energy Society. Published by Elsevier Ltd. All rights reserved.

Brus et al., 2015). This indicates that the non-intentional doping concentrations in the semiconductor active layer determine the band bending in the solar cell. Hence, a detailed understanding of the device electrostatic which is given by an initial charge carrier distribution at the internal donor-acceptor heterojunction is necessary.

Further, recent findings showed that the experimentally detected band bending in organic heterojunctions and metal/semiconductor junctions can be explained by initial diffusion of charge carriers from/into (depending on the work function) energetically distributed localized states (energetic disorder). Such diffusion implies Fermi level alignment and the formation of potential barriers (built-in potentials) at the material junctions (Gregg, 2009; Akaike et al., 2014; Lange et al., 2011; Oehzelt et al., 2014). Liu et al. proposed band bending to be a fundamental phenomenon promoting charge carrier collection in bilayer organic devices (Liu et al., 2008). In organic bulk heterojunction (OBHJ) devices, differences in charge carrier collection efficiency between standard and inverted solar cell architectures are well understood based on band bending (Dibb et al., 2013). Further, Deledalle et al. recently reported that a variation of the width of the space of charge region, which is responsible for band bending, strongly affects solar cell performance (Deledalle et al., 2015). More recently, Izawa et al. showed that band bending at the heterojunction affects $V_{oc}$ in bilayer organic solar cells, (Izawa et al., 2018). Also, Shintaku et al. demonstrated that intentional semiconductor doping controls $V_{oc}$ in organic solar cells (Shintaku et al., 2018). However, to the best of our knowledge such phenomena have not been considered in quantitative $V_{oc}$ analyses for organic solar cells.

Here, we show that a simple quantitative analysis of the dark conduction mechanisms and device electrostatics gives an accurate prediction of $V_{oc}$ in organic solar cells for the selective contacts case. It is consistent with both the $V_{bi}$ originating from a donor-acceptor abrupt (p-n$^{++}$) heterojunction, and the band bending phenomenon. Thus, we show that $V_{oc}$ is fundamentally limited by $V_{bi}$ at a donor-acceptor p-n$^{++}$ heterojunction.

Specifically, in this work, we study the current-voltage and capacitance-voltage characteristics of P3HT:PCBM OBHJ cells with ohmic contacts (Steim et al., 2010). We show that the thermionic emission mechanism describes the dominant recombination losses from which we can determine $V_{oc}$ at the potential barrier at the bulk donor-acceptor heterojunction interface. Further, we demonstrate that, analogous to inorganic or organic bilayer heterojunction devices, the potential barrier originates from the heterojunction electrostatics. Subsequently, we demonstrate that the typical experimentally observed $V_{oc}$ losses can be derived by using a band diagram in thermal equilibrium. The complete analysis demonstrates that $V_{bi}$ originates from a donor-acceptor abrupt (p-n$^{++}$) heterojunction. On this basis, the mechanism for charge collection at the heterojunction under different physical conditions is discussed. Subsequently, the generality of this analysis is confirmed using data from literature for both bulk and bilayer heterojunctions. Finally, we show that the dependence of $V_{oc}$ on the OBHJ cell contacts can be understood in terms of the potential barriers formed by the Fermi level alignment of non-intentionally doped semiconductors at all the junctions in the system.

## 2. Experimental part

The well-studied P3HT:PCBM system is analyzed in this work. Standard PEDOT(~50 nm)/P3HT:PC60BM(~100 nm)/Ca/Al solar cells were fabricated on pre-cleaned indium tin oxide (ITO) coated glass substrates. The cathode material was deposited by thermal evaporation at a pressure of $1 \times 10^{-6}$ mbar. All materials were used as received. The blend was prepared with a one weight percent of polymer in chlorobenzene, using a 2:1 ratio of polymer:fullerene. The organic film thicknesses were measured by atomic force microscopy. The devices possess an active area of 0.5 cm$^2$. The dark and illuminated current density-voltage ($J$-$V$) characteristics were measured using a Keithley digital source meter 2400. The $J$-$V$ curves recorded under illumination were obtained with a solar simulator (K. H. Steuernagel Technical Lightning) at an intensity of 100 mW/cm$^2$ (1 sun). The experimental $C$-$V$ data were measured at 50 kHz with a small signal of 50 mV, using an HP4194A impedance analyzer. The effect of deep (trap) states on the $C$-$V$ characteristics is an important fact to be considered in $C$-$V$ studies (Brus et al., 2015; Carr and Chaudhary, 2013). Typically, the effects of deeply trapped charges strongly manifest at relatively low frequency (Khelifi et al., 2011). Previously, for devices such as the ones studied here, we found that the charge concentration is usually constant over a range of intermediate frequencies (i.e. tens of kHz), whereas the extracted $V_{bi}$ value can depend on frequency. This has been attributed to interfacial trap states (Ecker et al., 2011). Thus, to validate $V_{bi}$ extracted from $C$-$V$ data, we compare it to the value calculated from the $J$-$V$ characteristics and with simulations in the 'Results and Discussion' section. The temperature measurements were carried out in a cryostat with a K-20 temperature controller.

## 3. Theory

Earlier, it was believed that the organic systems were intrinsic, however, the carrier concentration (~$1 \times 10^{16}$ cm$^{-3}$) obtained in dark by capacitance-voltage characteristics correspond to a doped system. This fact has led to the use of the term "non-intentional doping" in OBHJ solar cells (Deledalle et al., 2015). In this work we use the terminology for intentional doped semiconductors, such as n$^{++}$.

The open circuit voltage $V_{oc}$ in a solar cell is derived from the balance of photogeneration and recombination of charge carriers. This balance is generally quantified by the energetic difference between the quasi-Fermi levels of the electron and hole populations in the system (Tress, 2015; Tress et al., 2011). However, the maximum value of $V_{oc}$ that can be achieved without significant charge extraction losses is limited by built in electric fields (Fahrenbruch and Bube, 1983; Rau et al., 2003; Archer and Green, 2015). Thus, in this work we apply a theory which has been used to explain electrical phenomena occurring in organic devices involving such built in electric fields caused by non-intentional doping phenomena (Nolasco et al., 2010, 2014).

### 3.1. J-V characteristics

The physical phenomena occurring in electronic devices can be analyzed by means of electrical circuits. Here, we use an equivalent circuit which is shown in the inset of Fig. 1. Each branch of the circuit includes a diode, a shunt, and a series resistance ($R_p$ and $R_s$), respectively. The current in each one of the branches is given by the well-

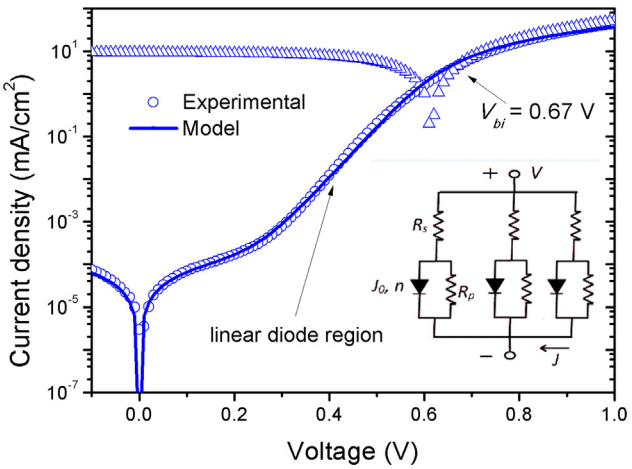


**Fig. 1.** Experimental illuminated, dark (open triangles, open circles) and modeled dark $J$-$V$ characteristics (solid line) of P3HT:PCBM solar cells. Inset: Electrical equivalent circuit.

known equation

$$J = J_0\left[\exp\left[\frac{q(V - JAR_S)}{nkT}\right] - 1\right] + \frac{V - JAR_S}{R_pA} \quad (1)$$

where $k$ is Boltzmanńs constant, $T$ the temperature, and $A$ the active area of the device. $n$ and $J_0$ are the ideality factor and the saturation current density of the diode, respectively. The values of $n$ and $J_0$ depend on the current recombination mechanisms in the device. The formation of potential barriers at Schottky metal/semiconductor and semiconductor/semiconductor junctions gives rise to the rectification properties. Generally, rectification in such junctions has been described by either drift-diffusion mechanisms (Würfel et al., 2015; Rhoderick, 1972) or by dominant thermionic emission of the charge carriers over the barrier, from the region with higher doping to the region with lower doping (Bethe, 1942). These mechanisms occur in series, and, as a result, the current is determined by the contribution with the largest impediment to the flow of charge. Earlier, Rhoderick argued that the thermionic emission theory proposed by H. Bethe for crystalline materials would also hold for low mobility materials when the quasi-Fermi level is sufficiently flat through the depletion region with carriers losing their potential energy at the interface. In contrast, when recombination is significant in the depletion region, the drift-diffusion model describes more accurately the electrical behavior (Tress, 2015; Würfel et al., 2015). Recently, we showed that thermionic emission theory can accurately describe the Schottky polymer/cathode potential barrier limiting $V_{oc}$ in OBHJs with non-ohmic cathode contacts (Nolasco et al., 2014). Here, we apply such a theory to a P3HT:PCBM bulk donor-acceptor heterojunction. Note that this theory has been consistently applied not only to Schottky type junctions but to inorganic semiconductor heterojunctions (Milnes and Feucht, 1972).

It is important to note that Eq. (1) is a non-ideal general diode expression, and that the ideal Shockley model corresponds to a specific case only, i.e., when $n = 1$ and $J_0$ is determined by band-to-band recombination of the minority carriers (Sze and Ng, 1979). For the case of ideal thermionic emission, $n = 1$, and $J_0$ is determined by the generation/recombination of majority carriers at a junction barrier. According to thermionic-emission theory, $J_0$ is given by

$$J_0 = A^*T^2\exp(-q\Phi_b/kT), \quad (2)$$

where $A^*$ (120 A/cm$^2$K$^2$) is the effective Richardson coefficient and $\Phi_b$ is the potential barrier height at the junction, e. g., the Schottky metal/semiconductor junction or the abrupt (i. e., there is a large difference in the doping density between the p and the n regions) semiconductor/semiconductor junction (heterojunction) (Milnes and Feucht, 1972; Sze and Ng, 1979). The fraction of carrier recombination which results in non-ideal $n$ values can be caused by additional mechanisms, such as trap assisted recombination (Hawks et al., 2014; Rau et al., 2000; Wetzelaer et al., 2011). Thus, depending of device's ideality factor, such contributions can become significant or even dominant under certain applied voltage, illumination or temperature conditions (Kirchartz et al., 2013).

By studying the temperature dependence of the saturation current $J_0$ in organic bilayer solar cells, Perez et al. (2009) proposed that $V_{oc}$ is determined by the activation energy at the interface given by $E_{D\text{-}A}/2$, while Potscavage et al. (2008) proposed that $V_{oc}$ is determined by a barrier formed at the heterojunction interface given by $mE_{D\text{-}A}$, where $m$ is an empirical factor that accounts for vacuum level misalignments and charge transfer states at the heterojunction. Also studying $J_0$, Waldauf et al. (2006) showed the relation between $V_{oc}$ and $E_{D\text{-}A}$ in OBHJ solar cells. However, all above studies consider no Fermi level alignment at the heterojunction and consequently a constant electric field in equilibrium defined by the difference between the work functions of the contacts. In this work, we explore the relation between $J_0$ and $V_{oc}$ using a theory that considers such a Fermi level alignment and consequently band bending.

Previously, we demonstrated that, for non-ohmic contact cathodes, the dependence of $V_{oc}$ on the cathode work function can be predicted by

$$V_{oc} = n\Phi_b - \frac{nkT}{q}\ln\left(\frac{A^*T^2}{J_{sc}}\right) \quad (3)$$

This equation was obtained by substitution of Eq. (2) into Eq. (1), once adding $J_{sc}$, considering open-circuit conditions (J = 0), and neglecting the last term in Eq. (1) due to high $R_p$ values (Nolasco et al., 2014; Castro-Carranza et al., 2016). A limitation of this model would become relevant for relatively low $R_p$ and high $R_s$ values, for which the last term in Eq. (1) cannot be neglected. One way to corroborate low $R_s$ values will be shown in the 'Results and Discussion' section.

Essentially, Eq. (3) differs from $V_{oc}$ expressions found in literature with regard to the following points: (i) considering an abrupt junction as the origin of charge separation and collection (Perez et al., 2009; Potscavage et al., 2008; Credgington and Durrant, 2012; Koster et al., 2005; Vandewal et al., 2010), (ii) taking into account $n$ in both terms of the equation (Fahrenbruch and Bube, 1983; Archer and Green, 2015), and (iii) considering thermionic emission of majority carriers toward the junction interface as the predominant recombination mechanism (Perez et al., 2009; Potscavage et al., 2008; Credgington and Durrant, 2012; Koster et al., 2005; Vandewal et al., 2010).

Thermionic emission considers the superposition of two current fluxes in opposite directions, one from the metal (or from the semiconductor with the highest carrier concentration for a heterojunction case) to the semiconductor and the other from the semiconductor to the metal (Bethe, 1942; Milnes and Feucht, 1972). While the first flux originates from the thermionic emission of electrons from the Fermi level of the metal and is not affected by the applied voltage, the second flux, arising from the thermionic emission of majority carriers at the semiconductor heterojunction, is influenced by the applied voltage via the resulting variations of the space charge region and consequently of band bending. The application of this theory to the internally distributed donor-acceptor heterojunction will be detailed later.

### 3.2. C-V characteristics

This technique can be used to derive important electrical parameters in a junction, i. e., the charge carrier concentration and $V_{bi}$ (Sze and Ng, 1979). In general, experimental *C-V* measurements in OBHJ cells have been interpreted in two different ways. One way has been modeling the system as an intrinsic effective medium (MIM model), the second considering only the depletion zone or space charge region (SCR) as formed at the polymer/cathode junction (Kirchartz et al., 2012). In both approaches, the internal donor-acceptor heterojunction has not been taken into account, although it gives rise to the photovoltaic phenomena in OBHJ. To include the heterojunction interface in the *C-V* interpretation, we use an alternative approach which we previously introduced. It consists in studying the system as a planar bilayer heterojunction (Ecker et al., 2011). Charge carrier concentrations are extracted from experimental *C-V* curves. *C-V* numerical simulations are used to corroborate the extracted parameters. Finally, a band diagram is calculated. The details about parameter extraction and simulations are included as Supplementary information.

## 4. Results and discussion

### 4.1. Analysis of the J-V characteristics

Fig. 1 shows the illuminated and dark *J-V* curves of the solar cells investigated in this study. The photovoltaic parameters ($V_{oc}$ = 0.6 V, short circuit current $J_{sc}$ = 9 mA/cm$^2$, and fill factor *FF* = 0.6) result in an efficiency of 3.2%, which lies within the range of the state of the art for the P3HT:PCBM system (Kniepert et al., 2014). To analyze the solar cells, we start with a three-blocking-junctions model for mobile

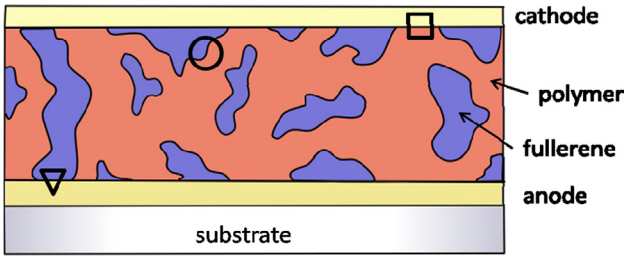


**Fig. 2a.** Schematic transversal view of an OBHJ solar cell. The three junctions in the system are: (i) the internally distributed polymer/fullerene heterojunction (circle), (ii) the polymer/cathode junction (square), and (iii) the fullerene/anode junction (triangle).

majority carriers (Snaith et al., 2004) (holes in the polymer phase and electrons in the fullerene phase, respectively) in dark. These junctions, illustrated in Fig. 2(a), are (i) the internally distributed polymer/fullerene heterojunction (circle), (ii) the polymer/cathode junction (square), and (iii) the fullerene/anode junction (triangle). The Schottky organic/metal junctions correspond to direct paths from the anode to the cathode of the polymer and the fullerene, respectively. A schematic of the band diagram (under non-equilibrium conditions) considering the $V_{bi}$ is shown in Fig. 2(b). Illumination causes a non-equilibrium situation (quasi-Fermi level splitting) by creating electron-hole pairs. These charge carriers can drift as caused by built-in potentials in the junctions and reach the respective contact, or recombine at the three junction interfaces. Non-intentional doping in organics has been attributed to the energetic disorder or defect states. These states can originate from intrinsic (covalent and non-covalent) or extrinsic defects (caused by synthesis and device fabrication) and can be present in any organic semiconductor (Gregg, 2009). Thus, band bending by action of non-intentional doping will be caused at all of the three junctions.

Further, on the basis of classical solid state semiconductor device theory, the $V_{bi}$ at the junctions is given by the difference in work function of the materials and corresponds to band bending at the polymer-cathode (i), polymer-fullerene (ii) and fullerene-anode interfaces (iii). In thermal equilibrium, at polymer-fullerene heterojunction, the barrier height ($\Phi_b$) is given by $V_{bi}$ and the energetic difference between the lower doping semiconductor transport band and its Fermi level. It will be detailed later for our P3HT:PCBM system. Under non-equilibrium conditions, i. e. under illumination and at certain applied voltages ($V_{applied}$) below $V_{bi}$, charge carriers drift to the respective electrodes due to the built-in potential in all junctions (electrons to the cathode and holes to the anode, as indicated in Fig. 2(b). Under $V_{oc}$ conditions, ideally, all charge carriers recombine at one of the device junctions only.

The current through the entire circuit (Fig. 1) corresponds to the sum of the current contributions from each branch. The dominant contribution of one branch to the total current manifests itself in a single slope at intermediate voltage (diode region) in semi-log dark *J-V* characteristics. We observe a single slope in the intermediate voltage region ($0.3\,V < V < 0.60\,V$ in this work, see Fig. 1), indicating the predominance of one junction at room temperature (Waldauf et al., 2006). In case of significant additional recombination mechanisms, regions with different slopes leading to ideality factors even higher than two are also observed within the same voltage region (Hawks et al., 2014). Considering that the open circuit voltage condition at 1 sun is reached in the diode region, and if the *J-V* characteristics of a solar cell obey the superposition principle, one expects that the recombination mechanisms resulting in $J_0$ will be similar under dark and illuminated conditions (Lindholm et al., 1979). This is because the photogenerated current is predominantly independent of the applied voltage, and the dark diode current is not affected by illumination. Therefore, the total current in the cell under illumination can be modeled by Eq. (1) shifted to the fourth quadrant by $J_{sc}$. One simple way to corroborate this approach is first to verify a reasonably high FF ($\sim > 0.6$) in the device which is an indication of a weak dependence of the photocurrent on the voltage. To verify that the dark current is not affected by illumination, dark and illuminated *J-V* characteristics are superimposed to confirm the overlap of both curves at voltages higher than $V_{bi}$. This $V_{bi}$ value is obtained when photocurrent becomes zero (Waldauf et al., 2006) and corresponds to the point where the curve under illumination superposes the dark *J-V* curve beyond $V_{oc}$ (see Fig. 1). Since a high potential drop over $R_s$ can lead to an overestimation of the $V_{bi}$ value (Street et al., 2011), we calculate the distribution of the applied voltage within the device determined by one branch of the equivalent circuit in dark conditions (Kanicki, 1992). Fig. 3 shows the voltage drop at the junction and at the resistance as a function of the applied voltage. One can note that at $V_{bi}$, the voltage at the resistance, amounts to 6% of the applied voltage. In addition, as expected from the superposition principle, a steep slope of the photocurrent at the crossing of the voltage axis is observed (see inset of Fig. 3), characteristic of low series resistance values (Street et al., 2011). These calculations demonstrate that the potential drop over $R_s$ can be reasonably neglected in the $V_{bi}$ estimation. Certainly, superposition is an ideal limit case since all the junctions in real devices possess an associated series resistance which can increase with the sample thickness (Cheyns et al., 2008).

Typically, a high FF correlates with both a $V_{oc}$ value close to $V_{bi}$ and *n* approaching 1 (Guo et al., 2013), since additional recombination mechanisms have a low impact on $V_{oc}$. This is consistent with the flatness of the quasi-Fermi level at the depletion zone. Further, our samples exhibit a relatively high FF, and a good overlap between the

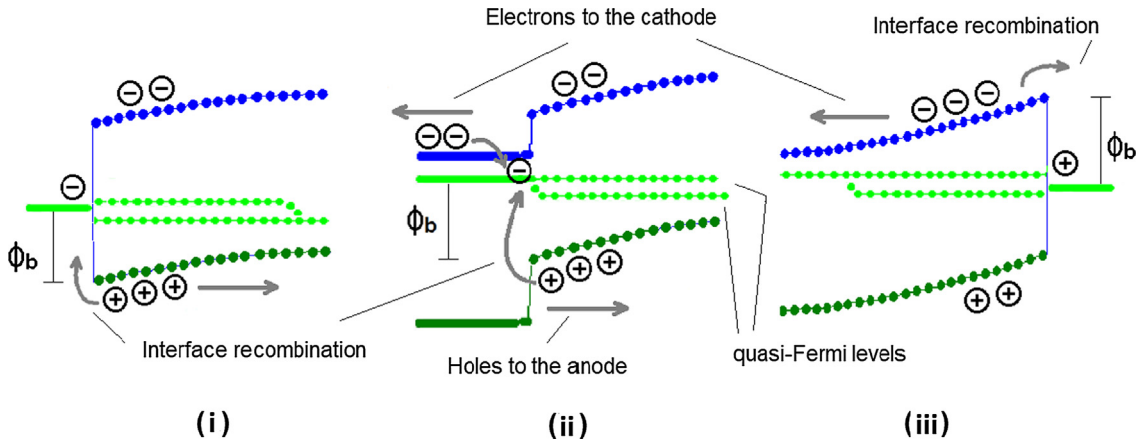


**Fig. 2b.** Schematic of the junction band diagrams at $V_{applied} < V_{bi}$ and illumination condition. The barrier height, the charge carrier collection and the recombination are indicated at the polymer/cathode junction (i), the polymer/fullerene heterojunction (ii), and the fullerene/anode junction (iii).

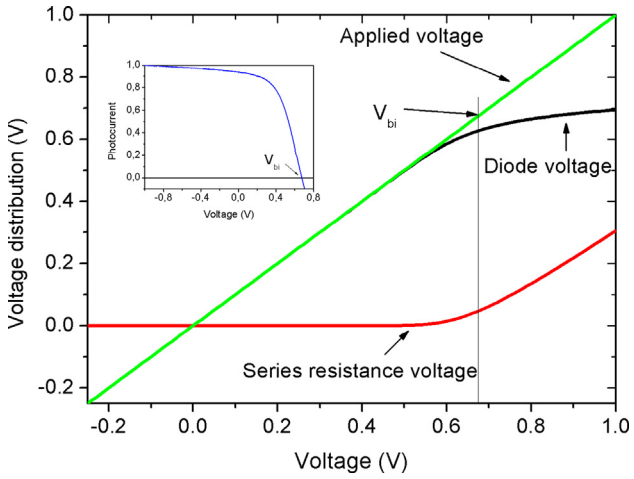


**Fig. 3.** Voltage drop of diode and series resistance as a function of applied voltage. At $V_{bi}$ the drop due to the resistance amounts to 6% of the total applied voltage. Inset: Normalized photocurrent exhibits a steep slope around the $V_{bi}$.

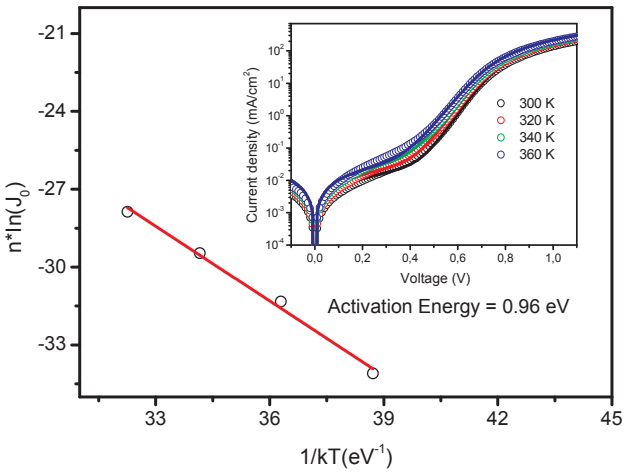


**Fig. 4.** Corrected (open symbols) Arrhenius plot of $J_0$. The activation energy is calculated by fitting Eq. (2) (line) considering the correction of $n$. Inset: Experimental (open circles) and modeled $J$-$V$ characteristics (solid lines) of P3HT:PCBM solar cells in dark at different temperatures.

dark and light $J$-$V$ curves is observed after reaching $V_{bi}$. Next, we fit the dark $J$-$V$ curve using Eq. (1). To avoid inconsistencies in the parameter extraction, $J_0$ and $n$ were first calculated from the intersection and from the slope of the linear diode region (see Fig. 1), respectively. The contributions of $R_p$ and $R_s$ dominate in the low ($0\,V < V < 0.3\,V$) and high ($0.67\,V < V < 1\,V$) voltage regions, respectively. The values of the extracted parameters were found to be $J_0 = 3.08 \times 10^{-10}\,A\,cm^{-2}$, $n = 1.4$, $R_p = 9 \times 10^5\,\Omega\,cm^2$, $R_s = 4.59\,\Omega\,cm^2$.

Here, we used Eq. (3) to verify that in the case of ohmic contacts, recombination at the internal donor-acceptor heterojunction dominates and that the recombination mechanism determining $J_0$ is the same under dark and illumination conditions. For this purpose, we first calculated $\Phi_b$ using Eq. (3) and compared the result to values from literature, specifically to the activation energy (0.93 eV (Waldauf et al., 2006), 1.07 eV (Foertig et al., 2012) for charge recombination at the heterojunction obtained by temperature-dependent $J_0$ analysis, and to an $E_{CT}$ value of 1.08 eV determined by external quantum efficiency characteristics (Vandewal et al., 2008). From our data we obtained a $\Phi_b = 0.98$ eV. Second, a value for $J_0$ under illumination was calculated using $\Phi_b$ (determined from the illuminated solar cell parameters and using the dark $n$ which is independent of $J_0$ in the parameter extraction procedure) and Eq (2). $J_0$ is found to be $3.84 \times 10^{-10}\,mA\,cm^{-2}$ which is comparable to the value of $3.08 \times 10^{-10}\,mA\,cm^{-2}$ extracted from the dark $J$-$V$ characteristics. *The good agreement between these values confirms both, the dominance of interface recombination at the internal donor-acceptor abrupt junction resulting in $J_0$ in the case of an ohmic cathode, and $J_0$ being the same under dark and illumination conditions considering that n is extracted in dark.*

To further verify the above results, we calculated the activation energy of $J_0$ from temperature dependent $J$-$V$ characteristics. Operation temperatures above room temperature, i. e., for which charge collection is relatively constant (Hörmann et al., 2013; Riedel et al., 2005) were analyzed. For a non-ideal mechanism which corresponds to the case studied here, the typical method to determine the activation energy from a $J_0$ temperature analysis considering $n$ is using an Arrhenius modified curve, i. e., considering the product $n^*J_0$ instead of simply $J_0$ (Archer and Green, 2015; Hörmann et al., 2013). This curve for the P3HT:PCBM device is shown in Fig. 4. The origin of $n$ values higher than one will be discussed later. Consistently, we find that the obtained barrier, 0.96 eV, corresponds to the one calculated above using Eq. (3) yielding 0.98 eV.

Variations in $n$ have been related to the morphology of the blend (Waldauf et al., 2006). It has already been shown that Eq. (3) is valid for devices with $n$ values between 1 and 2 (Nolasco et al., 2014). In thin film solar cells, in general, the origin of additional recombination determining $n$ has been attributed to recombination within the bulk space charge region or at the heterojunction interface region. In the space charge region, it has been described by the Shockley-Read-Hall (SRH) mechanism along with tunneling (Rau et al., 2000) or simply by SRH recombination (Hawks et al., 2014; Blakesley and Neher, 2011). Meanwhile $n$ has been described at the interface by tunneling enhanced interface recombination (Rau et al., 2000). These mechanisms consider a distribution of localized states. The temperature analysis of $J_0$ in bilayer organic solar cells (Nolasco et al., 2010) and in the present work are consistent with tunneling enhanced interface recombination to define the origin of the $n$ values.

Taking into account that, in the second term of Eq. (3), the linear temperature dependence dominates the logarithmic one, the typical linear dependence of $V_{oc}$ on temperatures close to room temperature in OBHJ (Gélinas et al., 2014; Riedel et al., 2005, 2004; Garcia-Belmonte, 2010) is well predicted. This equation also describes the well-known linear relation between $V_{oc}$ and the logarithm of the light intensity (Riedel et al., 2004). A third method to calculate $\Phi_b$ consists in extrapolating the linear region of $V_{oc}$ versus temperature to T = 0, yielding $n^* \Phi_b$. Thus, according to Eq. (3), $V_{oc}$ does not reach values of $n^* \Phi_b$ completely for temperatures above 0. This agrees with the ZnPc:$C_{60}$ system with ideality factors approaching one (Widmer et al., 2013). Less ideal systems, e. g., those with relatively high ideality factors (approaching to 2) and low FF (at room temperature), have shown a change in the slope in the $V_{oc}$ versus T characteristics below room temperature (Hörmann et al., 2013; Riedel et al., 2005; Koster et al., 2005) which is not predicted by Eq. (3) if $n$ is extracted in dark. Additionally, a saturation effect that can shift to relatively high temperatures and that depends on the light intensity (Vandewal et al., 2010; Rauh et al., 2011) along with an increment of the ideality factor (Hörmann et al., 2013; Riedel et al., 2005) and an increment of collection losses (Riedel et al., 2004) has been observed in such systems at low temperatures. Thus, in this case, the linear region above room temperature and 1 sun conditions should be considered to extract $\Phi_b$. In addition, the $V_{oc}$ saturation effect at low temperatures in *OBHJs* has been attributed to the $V_{bi}$ caused by the contacts (Rauh et al., 2011).

In summary, the above result indicates majority carrier recombination occurring at the heterojunction barrier being the dominant recombination mechanism.

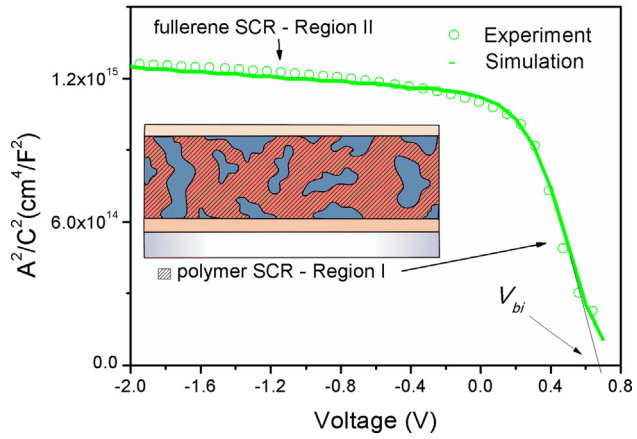


**Fig. 5.** Experimental (symbol) and simulated (line) capacitance-voltage characteristics of the P3HT:PCBM solar cell. Inset: A sketch of the fully depleted P3HT phase (hatch patter) in equilibrium.

### 4.2. Capacitance-voltage characteristics analysis

We applied C-V measurements to verify that $\Phi_b$, which up to now has just been considered in context of flat bands at the interface heterojunction in OBHJ in literature (Perez et al., 2009; Potscavage et al., 2008; Waldauf et al., 2006), is related to the electrostatics of the system in thermal equilibrium as expected from thermionic emission theory.

The experimental *C-V* curve is displayed in Fig. 5. As previously observed in bilayer organic and in OBHJ solar cells (Ecker et al., 2011; Nolasco et al., 2010), the curve exhibits two regions with different slopes. Region I at medium positive voltage (diode region) has been attributed to a SCR in the P3HT absorber. The non-saturated region, observed at negative voltage (Region II), has been assigned to a SCR in the PCBM absorber (Ecker et al., 2011). The typical observation of such a non-saturated region in inorganic heterojunction solar cells led to its modeling (Chopra and Das, 1983). In the present case, Region II is observed when the P3HT layer is fully depleted (around 0 V). A sketch of the fully depleted P3HT phase in equilibrium is included as inset in Fig. 5. $V_{bi}$, the charge concentration $N_{P3HT}$ in the P3HT layer, and that in the PCBM layer ($N_{PCBM}$) were extracted as indicated in Refs. Ecker et al. (2011) and Nolasco et al. (2010); see also the Supplementary information. The obtained values are $N_{P3HT} = 1.6 \times 10^{16}\,cm^{-3}$; $N_{PCBM} = 1 \times 10^{18}\,cm^{-3}$, and $V_{bi} = 0.68$ V, which is consistent with a (p-n$^{++}$) abrupt heterojunction. The values for the charge carrier concentration in P3HT and in fullerene agree with those reported for single-layer devices (Carr and Chaudhary, 2013) and bilayer heterojunctions (Nolasco et al., 2010), respectively, being extracted from capacitance measurements. The P3HT charge concentration is also in agreement with results from charge extraction methods (Rauh et al., 2011), the consistency of the PCBM charge carrier concentration with those got from other methods will be demonstrated below. $V_{bi}$ is in agreement with the value obtained from the *J-V* characteristics (0.67 eV, see Fig. 1), *confirming that $V_{bi}$ extracted from the C-V characteristics is determined by the internal* donor-*acceptor heterojunction.* The differential capacitance technique can be used independently of the geometry of the junction interface. Using Schottky junctions, Goodman (1963) showed that geometric variations of the surface area in the order of magnitude of the SCR width result in parabolic shapes of the *C-V* curves. In this case, it is not possible to simply calculate the charge concentration from the linear section of the *C-V* characteristics. Thus, the linear behavior observed in the regions I and II indicates that shape variations of the distributed donor-acceptor heterojunction interface are significantly smaller than the SCR width of such regions, and that the planar approximation can be used.

### 4.3. C-V characteristics and numerical simulations of the heterojunction band diagram

The extracted charge concentration and material energetics, taken from values in literature, ($LUMO_{P3HT} = 3.3$ eV, $HOMO_{P3HT} = 5.2$ eV, $\varepsilon_{P3HT} = 3$, $LUMO_{PCBM} = 4.05$ eV, $HOMO_{PCBM} = 5.87$ eV, $\varepsilon_{PCBM} = 2.4$) (Khelifi et al., 2011; Kim et al., 2006; Xu et al., 2009) were used to simulate the *C-V* characteristics of a planar heterojunction using a numerical heterojunction semiconductor software (AFORST-HET) (Schmidt et al., 2007). The simulated characteristics (solid line) in Fig. 5 show a good agreement with the experimental characteristics based on an effective layer thicknesses of 90 nm and 25 nm for P3HT and PCBM, respectively. The P3HT thickness is comparable to the thickness of the active layer (~100 nm) and the PCBM layer thickness corresponds to the size of the PCBM domains (~20 nm) (Hoppe and Sariciftci, 2006). This result also indicates that the vertical junctions (polymer/fullerene and polymer/cathode) in Figs. 2 determine the SCR regions due to direct paths from the anode to the cathode of the polymer, and not of the fullerene, are formed. Note that it has been observed that region II in the *C-V* characteristics is sensitive to the concentration of PCBM in the blend (Boix and Garcia-Belmonte, 2009), presumably due to an increment in PCBM domain size, which agrees with the bilayer heterojunction approach. Note also that in thin film solar cells, it has been demonstrated that the depletion approximation holds at positive voltages (Chopra and Das, 1983). This is verified here by simulating *C-V* characteristics of the heterojunction with different donor layer thickness using the material parameters given above. The simulations are shown in Fig. 6. As expected, due to the dependence of the SCR on the applied potential, the same slope at both positive and negative voltages is observed for all thicknesses using a mobility of 0.01 $cm^2/V\,s$ (Hawks et al., 2014). We note that as long as the absorber is totally depleted at V = 0 V, the *C-V* characteristics are independent of carrier mobility which is consistent with the negligible effect of $R_s$ on $V_{bi}$. Thicker samples along with low mobility materials would result in a high $R_s$ affecting the *C-V* characteristics, therefore requiring further data correction (Straub et al., 2005).

We calculated a band diagram to facilitate the analysis of the heterojunction using the material properties from the modeling of the experimental *C-V* measurements and AFORST-HET. The charge carrier concentrations having been extracted from *C-V* characteristics and attributed to localized states associated to energetic disorder (Hawks et al., 2014; Ripolles et al., 2013; Blakesley and Neher, 2011) can be introduced to the simulator as effective doping densities to calculate the

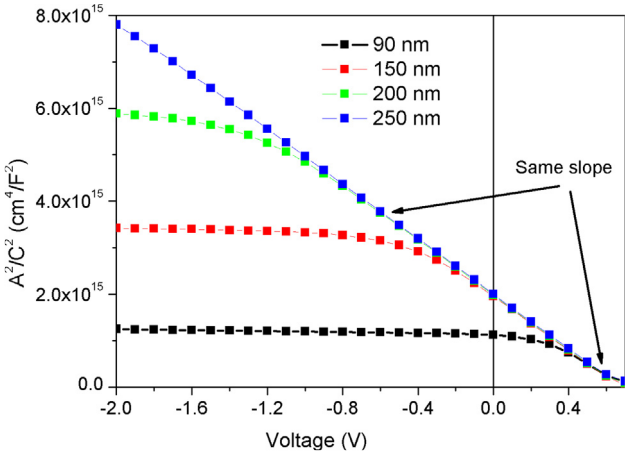


**Fig. 6.** Simulated capacitance-voltage characteristics of the P3HT/PCBM heterojunction for different P3HT thicknesses. The validity of the depletion approximation at positive voltage for the determination of the charge carrier concentration is verified with simulation. The same slope at Region I for all the characteristics can be noted.

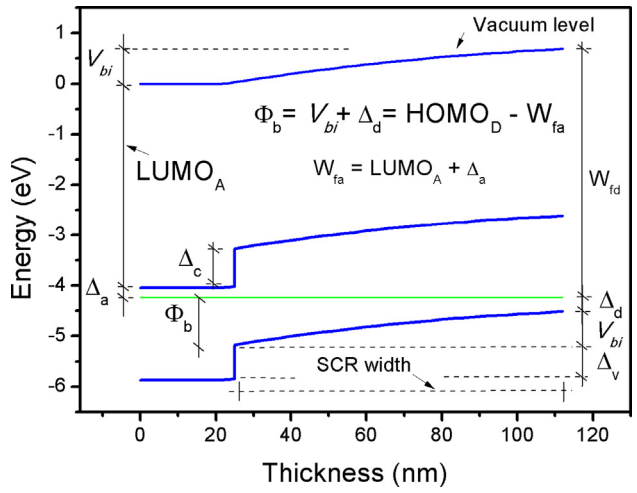


**Fig. 7.** Simulated band diagram of the P3HT/PCBM heterojunction in the OBHJ solar cell in thermal equilibrium.

heterojunction electrostatics (Liu et al., 2008; Gregg, 2009). The calculation essentially consists of solving the Poisson equation for the heterojunction. The corresponding diagram is shown in Fig. 7. The parameters used for the diagram describe potential energies, most of them are given/assumed relative to certain energy levels but some with regard the vacuum level (this is the level at which the charge carries do not experience any forces from the materials). Specifically, $LUMO_A$, $LUMO_D$ $HOMO_A$, $HOMO_D$ $W_{fa}$, and $W_{fd}$ (the latter levels correspond to the work functions of the acceptor and the donor, respectively) are given with regard to the vacuum level. Meanwhile, $\Delta_c$, $\Delta_v$, $\Phi_b$, $V_{bi}$, $\Delta_a$ and $\Delta_d$ values are given relative to $LUMO_A$, $HOMO_D$, $W_{fa}$, and $W_{fd}$, respectively. In thermal equilibrium, Fermi level aligment occurs (in green in Fig. 7) and the value of the vacuum level changes since the HOMO and LUMO levels must keep constant. This vacuum level variation corresponds to $V_{bi}$ which is determined by the difference between the work functions of the materials. These work functions correspond to the energies required to release charge carriers from the Fermi level to the vacuum level and depend on the non-intentional dopants' concentrations in the materials. The LUMO and HOMO level discontinuities ($\Delta_c$ and $\Delta_v$, where $\Delta_c = |LUMO_A - LUMO_D|$ and $\Delta_v = |HOMO_A - HOMO_D|$) as well as $V_{bi}$ are the relevant parameters to drive the charge carriers to their corresponding electrode at the heterojunction (see Fig. 2b).

According to thermionic emission theory, $\Phi_b$ is given by the difference between the Fermi level of the metal and the majority carrier band in the junction. In thermal equilibrium, $\Phi_b$ equals to the sum of q $V_{bi}$ and $\Delta_d$, where $\Delta_d$ is the difference between the edge of the majority carrier band and the Fermi level of the semiconductor. In a semiconductor/semiconductor junction, a potential barrier is formed in the material with the significantly lower charge concentration. In the case of a polymer/fullerene junction, the barrier height in equilibrium would correspond to the sum of $q{\cdot}V_{bi}$ and $\Delta_d$ in the polymer (donor), as indicated in Fig. 7. $\Delta_d$ can be obtained using the well-known Boltzmann expression, i. e., $\Delta_d = kT * \ln (N_c/N_{P3HT})$, where $N_c$ is the effective density of states in the valence band. Applying $N_{P3HT}$ and $V_{bi}$ from *C-V* characteristics, $N_c = 1 \times 10^{21}\,cm^{-3}$, $\Phi_b = 0.96$ eV ($q{\cdot}V_{bi} = 0.68$ eV, $\Delta_d = 0.28$ eV) were obtained. *The good agreement between this barrier value and the one derived from the J-V analysis (0.98 eV) demonstrates the barrier to be related to the heterojunction electrostatics, as expected from the theory*. This result is consistent with our previous analysis on a planar heterojunction (Nolasco et al., 2010). $\Delta_a$ indicated in Fig. 7, related to the charge concentration in the fullerene (acceptor), was calculated by $\Delta_a = kT * \ln (N_c/N_{PCBM})$, yielding $\Delta_a = 0.18$ eV. From the band diagram, the work function of the fullerene $W_{fa}$ was determined as $W_{fa} = HOMO_D - \Phi_b$. Using the literature value of $HOMO_D$ (5.2 eV (Kim et al., 2006) and $\Phi_b$, we end up with $W_{fa} = 4.23$ eV. This value agrees with that determined by ultraviolet photoelectron spectroscopy (UPS, 4.3 eV (Xu et al., 2009). $\Delta_a$ lies also within the range of energies (0.045 eV − 0.184 eV) found for PCBM using thermally stimulated current (Credgington and Durrant, 2012; Schafferhans et al., 2011). This confirms the consistency of the PCBM charge concentration obtained by capacitance characteristics. Note that all the HOMO values from literature considered in this study were obtained by cyclic voltammetry, and that the values calculated by UPS correspond to the Fermi level of the respective material (Cahen and Kahn, 2003).

We will now focus on $V_{oc}$ losses and their relation with $V_{bi}$. From the diagram, we obtain $E_{DA} = q{\cdot}V_{bi} + \Delta_d + \Delta_a$. Assuming that $V_{bi}$ corresponds to the maximum value of $V_{oc}$ at 1 sun condition, the difference between these values, denoted by $\Delta_e/q$, amounts to 0.08 V. Inserting $\Delta_e$ and considering that $\Delta_d$ and $\Delta_a$ do not change under illumination (consistent with devices obeying the superposition principle) the latter relationship can be rewritten as

$$E_{DA} - q{\cdot}V_{oc} = \Delta_d + \Delta_a + \Delta_e, \quad (4)$$

which yields 0.54 eV. This value agrees with the typical $V_{oc}$ losses in organic solar cells (~0.55 eV (Vandewal et al., 2014; Widmer et al., 2013). We can also quantify $V_{oc}$ losses in terms of the absorber band gap ($E_{G\text{-}A}$) by using $E_{DA} = E_{G\text{-}A} - \Delta_C$ from the diagram, where $\Delta_C$ is the difference of LUMO values in the heterojunction. Thus, taking the corresponding $\Delta_C$ value (0.75 eV), $E_{G\text{-}A} - q{\cdot}V_{oc} = 1.36$ eV is obtained, which is also in agreement with the ranges reported in literature (from 0.7 to more than 1.1 eV (Graham et al., 2013). Moreover, considering the Fermi level of the fullerene to be approximately equal to its LUMO level (Scharber et al., 2006), $E_{DA} - q{\cdot}V_{oc}$ amounts to 0.36 eV which corresponds to a factor of 0.30, as proposed by Brabec et al. (2001). Eq. (4) agrees with $V_{oc}$ predictions made by Poelking et al. (2015), but here, we consider the macroscopic band bending in the cells. From Eq. (4), a reduction of $V_{oc}$ losses by lowering $\Delta_d$, $\Delta_a$, and $\Delta_e$ can be envisaged. However, to increase the efficiency of the cell, $\Delta_d$ should have an optimum value, since small $\Delta_d$ values resulting in a width of SCR lower than the device thickness can significantly reduce charge collection and consequently the FF and the $J_{SC}$ values of the device (Deledalle et al., 2015).

Specifically, $V_{bi}$ should be optimized having in mind that this parameter corresponds to the maximum $V_{oc}$ without charge extraction losses, and the maximum $V_{bi}$ is determined by a total depletion condition in the lowest non-intentional doping material which in turns depends on its dopant concentration. Thus, there is a competing effect: on the one hand $V_{bi}$ should be maximized by increasing $N_{P3HT}$ according to the following general equation, $V_{bi} = W_{fd} - W_{fa}$, where $W_{fd} = HOMO_{P3HT} - \Delta_d$, and $\Delta_d = kT * \ln (N_c/N_{P3HT})$; however, on the other hand, is an inverse relation between $N_{P3HT}$ and the SCR width that has to be taken into account (the respective equation is included in the Supplementary information). For the here studied system, our simulations indicate a highest value of $N_c = 2.8 \times 10^{16}\,cm^{-3}$ for the P3HT phase to be totally depleted, which implies a $\Delta_d = 0.27$ eV that will in turn correspond to a maximum $V_{bi} = 0.7$ V. The agreement of this value and the experimental one (0.68 V) can explain the relatively high collection efficiency of the P3HT:PCBM system.

Moreover, note that $V_{oc}$ cannot exceed $V_{bi}$ in case of non-selective contacts, and that $V_{oc}$ can be higher than $V_{bi}$ at certain illumination conditions higher than 1 sun in case of selective contacts. However, at this condition $V_{bi}$ is zero, thus recombination increases yielding a low FF. The condition $V_{oc} > V_{bi}$ can occur even at 1 sun and room temperature in devices with poor performance i. e. with high ideality factors and low FF. Thus, the collection efficiency of such devices increases at lower illumination. Note that although one of the materials is totally depleted the theory used in this work can be applied. In this case, a variation of the depleted layer thickness modifies the electric field which can affect charge collection (Izawa et al., 2018). In addition, the depletion zone depends on physical conditions, e.g. at illuminations

**Table 1**
Energy values of the ideal barrier obtained by Eq. (3) versus calculated values by the difference $HOMO_D - W_{fa}$ (4.23 eV (Xu et al., 2009) using literature data for five solar cells with different polymers and small molecules as donors. $V_{oc}$, $J_{sc}$, $n$, $HOMO_D$, and the weight ratio of the blends used for the solar cells are listed (Vandewal et al., 2009; Nolasco et al., 2010; Hörmann et al., 2013).

| Device | Eq. (3) $\Phi_b$(eV) | Diff. $\Phi_b$(eV) | $V_{OC}$ (V) | *Jsc* (mA·cm$^{-2}$) | *n* | $HOMO_D$ (eV)/Literature | Weight ratio (upper four)/Thicknesses (lower two) |
|---|---|---|---|---|---|---|---|
| LPPP5:PCBM | 1 | 1.03 | 0.73 | 4.5 | 1.53 | 5.3 Hellström et al. (2009) | (1:3) |
| MDMO:PCBM | 1.1 | 1.14 | 0.83 | 3.4 | 1.45 | 5.4 Thompson and Frechet (2008) | (1:4) |
| APFO3:PCBM | 1.2 | 1.21 | 1.02 | 4.5 | 1.56 | 5.5 Li et al. (2010) | (1:4) |
| Pc/$C_{60}$ | 0.85 | 0.91 | 0.45 | 5.6 | 1.6 | 5.1 Tang et al. (2006) | 40 nm/30 nm |
| 6T/$C_{60}$ | 0.82 | 0.87 | 0.41 | 2.3 | 1.7 | 5.1 Choi et al. (2013) | 40 nm/80 nm |

close to 1 sun the semiconductor is not totally depleted anymore, thus charge collection is affected. These results demonstrate that fundamental limitations in $V_{oc}$ can be identified by considering internal donor-acceptor heterojunction electrostatics, i.e., $V_{bi}$.

### 4.4. Generalization of the $V_{oc}$ model

In order to verify the generality of the analysis presented in this work, $\Phi_b$ was calculated for both OBHJ and organic planar heterojunction solar cells with ohmic contacts using. The solar cell materials and weight ratio or layers thickness are specified in Table 1. The experimental parameters such as $V_{oc}$, $J_{sc}$, $J_0$, and $n$, for the OBHJ devices were taken from Ref. Vandewal et al. (2009) and its Supplementary information. The planar heterojunction parameters were taken from Refs. Nolasco et al. (2010) and Hörmann et al. (2013). All calculations were performed for room temperature. $\Phi_b$ calculated using Eq. (3) is compared with the difference between $HOMO_D$ and $W_{fa}$ (4.23 eV). The $HOMO_D$ energy for each polymer or small molecule was taken from Refs. Hellström et al. (2009), Thompson and Frechet (2008), Li et al. (2010), Tang et al. (2006), Choi et al. (2013). The calculated barriers and the numerical values employed in the calculations are listed in Table 1. We note the good agreement between the $\Phi_b$ values predicted by Eq. (3) and the energy difference $HOMO_D - W_{fa}$. The largest deviation of $\Phi_b$ from the latter energy difference amounts to 0.06 eV. This deviation is in the range of typical experimental error variations (0.1 eV) (Hörmann et al., 2013) and in the range of possible room temperature variations during the electrical characterization. The latter considers that a variation in temperature of ± 10 °C in Eq. (3) results in a $\Phi_b$ variation of ± 0.06 eV. *These results support the generality of the present study*. The analyzed results are certainly not world records in efficiency; however, the low ideality factors of the devices indicate that they are relatively efficient.

We demonstrate that $V_{oc}$ can be predicted if the electrostatic picture of the solar cell is quantitatively understood. On this basis, at $V_{oc}$ conditions recombination effectively occurs at energies between $\Delta_d$ and $\Delta_a$. Thus, dissociation of charge carriers at $V_{oc}$ via release of charge carriers from localized to delocalized states take place. $\Delta_d$ and $\Delta_a$ are consistent with the Meyer-Neldel rule arising from the filling of localized states until the equilibrium is reach as observed in organic transistors under dark conditions (von Hauff and Parisi, 2006; Fishchuk et al., 2014). $\Delta_a$ (0.18 eV) is in agreement with the electrostatic energy arising from charge separation in fullerene aggregates (0.2 eV), calculated by Gelinas et al. (Gélinas et al., 2014) using ultrafast spectroscopy on OBHJ solar cells. This picture is also consistent with the charge relaxation to the $E_{CT}$ state before separation occurs, as proposed by Vandewal et al. (2014) and with the observed good correlation between $E_{CT}$ and $V_{oc}$ in fullerene based solar cells (Benduhn et al., 2017).

The present study raises the question of why the fullerene phase is non-intentionally heavily doped with regard to the non-intentionally doped polymer. This could be due to the deeper covalent intrinsic defects that generally exist in polymers (Gregg, 2009). This phenomenon implies that the Fermi level comes closer to the corresponding transport band in the fullerene only what will lead in turn to a higher non-intentional doping effect. Finally, the evidence of defect states brings us to infer that, at open-circuit conditions, charge non-radiative recombination of the charge carriers predominantly occurs through the ranges of the energies $\Delta_d$ and $\Delta_a$; and that $\Phi_b$ corresponds to the so-called lowest radiative recombination transition $E_{CT}$ (Hörmann et al., 2013). *Thus, all facts together indicate that $V_{oc}$ is limited by $V_{bi}$. Hence, to improve the solar cell efficiency, $V_{bi}$ should be increased as long as the condition of fully depletion in the material with the lowest doping concentration is met.*

### 4.5. Understanding selective and non-selective contacts on the basis of junctions' band bending

Finally, we address the question how the dependence of $V_{oc}$ on the work function of the device contacts can be understood based on our present analysis. Previously, we demonstrated that majority carrier recombination takes place at the potential barrier formed at the Schottky polymer/cathode junction in OBHJ cells in the case of non-ohmic cathodes, and that this recombination limits $V_{oc}$ (Nolasco et al., 2014). It has been found that independent of fabrication treatments and the nature of the contact, direct paths of the polymer phase from the anode to the cathode are formed (Campoy-Quiles et al., 2008). Thus, it is expected that such a polymer/cathode barrier is formed in devices with ohmic contacts, since it is a prerequisite for charge selectivity (Steim et al., 2010). However, since an ohmic contact (fullerene/cathode) is formed when the work function of the cathode material ($W_{fc}$) is lower or equal to $LUMO_A$, the interface barrier at the polymer/cathode junction is higher than the barrier at the heterojunction. More precisely, for an ohmic contact, $HOMO_D - W_{fc} > HOMO_D - LUMO_D$ holds. *Thus, we conclude that this situation results in the suppression of majority carrier recombination at the polymer/cathode interface contact under $V_{oc}$ conditions, since now the recombination of charge carriers at the internal* donor-*acceptor herojunction interface barrier, which is the lowest barrier in the system, dominates.* Further, the formation of a Schottky barrier at metal/fullerene interfaces given by the difference between the $LUMO_A$ and the metal is well demonstrated (Yang et al., 2013). Devices whose $V_{oc}$ is limited by the contact barriers typically possess relatively low $V_{oc}$ values which result in lower efficiencies (Sze and Ng, 1979). $V_{oc}$ limited by the anode was observed when a high concentration of fullerene is used in the blend (Zhang et al., 2011; Yang et al., 2014), and in small-molecule donor OBHJ solar cells (Tress et al., 2013). These facts indicate that losses in $V_{oc}$ caused by recombination at the barrier in the fullerene/anode junction become possible when direct paths of fullerene from the anode to the cathode are formed. Thus, we infer that Eq. (3) can predict $V_{oc}$ when majority carrier recombination predominates at any interface barrier. In this situation $\Phi_b$ corresponds to the lowest potential barrier in the system, which ultimately determines $V_{bi}$. This picture can also explain fundamental differences in $V_{oc}$ observed between OBHJ and bilayer devices (Uhrich et al., 2008), as the hole transport layer in OBHJ determines $V_{bi}$ at the anode/fullerene junction. Thus, the three junction model (Snaith et al., 2004) and considering band bending can explain the physical limitation of the $V_{oc}$ based on the energy levels of the materials. This $V_{oc}$ contact selectivity rule was initially described in terms of intrinsic semiconductors (Tress et al., 2013; Uhrich et al., 2008). We show that it is possible to

understand such a rule by considering Fermi level alignment of the non-intentionally doped semiconductors in the three OBHJ junctions including the internal donor-acceptor heterojuntion which corresponds to an abrupt (p-$n^{++}$) heterojunction.

## 5. Conclusions

In summary, combining experimental *J-V* and *C-V* data with analytical and numerical modeling we demonstrated that $V_{oc}$ in OBHJ efficient devices using non-intentionally doped semiconductors and ohmic contacts can be determined from the device electrostatics, therefore implying that $V_{oc}$ is ultimately limited by the built-in potential at an internal donor/acceptor abrupt (p-$n^{++}$) heterojunction. This agrees with the band bending phenomena observed in junctions involving organic semiconductors. The generality of our findings is confirmed by using our solar cells and standard devices reported in literature with different materials. We also showed that the dependence of $V_{oc}$ on the OBHJ device contacts, initially described in terms of intrinsic semiconductors, can be understood by considering the Fermi level alignment of the semiconductors at the abrupt heterojunction and at the Schottky junctions formed by the device contacts.

## Acknowledgements

J.C. Nolasco is indebted to the Alexander von Humboldt Foundation for providing the George Foster grant. A. Castro-Carranza acknowledges support from Universität Bremen/FP7-PEOPLE-2012 COFUND Marie-Curie Fellowship “BREMEN TRAC”, project no. 600411, and CONACYT Mexico. The authors also thank for the support obtained from the projects UNAM-PAPIIT IA 107517 and IA107417. J.C. Nolasco would also like to thank Dr. A Morales-Acevedo for his thoughtful discussion to make some ideas clear for this work.

## Appendix A. Supplementary material

Supplementary data to this article can be found online at https://doi.org/10.1016/j.solener.2019.04.031.

## References

Akaike, K., Koch, N., Oehzelt, M., 2014. Fermi level pinning induced electrostatic fields and band bending at organic heterojunctions. Appl. Phys. Lett. 105 (22) 223303-1-223303–4.

Archer, M.D., Green, M.A., 2015. Clean Electricity from Photovoltaics, 2nd ed. Imperial College Press, London.

Benduhn, J., Tvingstedt, K., Piersimoni, F., Ullbrich, S., Fan, Y., Tropiano, M., McGarry, K.A., Zeika, O., Riede, M.K., Douglas, J., Barlow, S., Marder, S.R., Neher, D., Spoltore, D., Vandewal, K., 2017. Intrinsic non-radiative voltage losses in fullerene-based organic solar cells. Nature Energy 2 17053(1)-17053(6).

Bethe, H.A., 1942. Theory of the Boundary Layer of Crystal Rectifiers. MIT Radiation Laboratory Report, 43, 12.

Blakesley, J.C., Neher, D., 2011. Relationship between energetic disorder and open-circuit voltage in bulk heterojunction organic solar cells. Phys. Rev. B 84 (7) 075210-1-075210-12.

Boix, P.P., Garcia-Belmonte, G., Muñecas, U., Neophytou, M., Waldauf, C., Pacios, R., 2009. Determination of gap defect states in organic bulk heterojunction solar cells from capacitance measurements. Appl. Phys. Lett. 95 (23) 233302-1- 233302–3.

Brabec, C.J., Cravino, A., Meissner, D., Sariciftci, N.S., Fromherz, T., Rispens, M.T., Sanchez, L., Hummelen, J.C., 2001. Origin of the open circuit voltage of plastic solar cells. Adv. Funct. Mater. 11 (5), 374–380.

Brus, V.V., Kyaw, A.K.K., Maryanchuk, P.D., Zhang, J., 2015. Quantifying interface states and bulk defects in high-efficiency solution-processed small-molecule solar cells by impedance and capacitance characteristics. Prog. Photovolt. 23 (11), 1526–1535.

Burke, T.M., Sweetnam, S., Vandewal, K., McGehee, M.D., 2015. Beyond Langevin recombination: how equilibrium between free carriers and charge transfer states determines the open-circuit voltage of organic solar cells. Adv. Energy Mater. 5 (11), 1500123.

Cahen, D., Kahn, A., 2003. Electron energetics at surfaces and interfaces: concepts and experiments. Adv. Mater. 15 (4), 271–277.

Campoy-Quiles, M., Ferenczi, T., Agostinelli, T., Etchegoin, P.G., Kim, Y., Anthopoulos, T.D., Stavrinou, P.N., Bradley, D.D.C., Nelson, J., 2008. Morphology evolution via self-organization and lateral and vertical diffusion in polymer: fullerene solar cell blends. Nature Mater. 7 (2), 158–164.

Carr, J.A., Chaudhary, S., 2013. The identification, characterization and mitigation of defect states in organic photovoltaic devices: a review and outlook. Energy Environ. Sci. 6 (12), 3414–3438.

Castro-Carranza, A., Nolasco, J.C., Reininghaus, N., Geißendörfer, S., Vehse, M., Parisi, J., Gutowski, J., Voss, T., 2016. Analytical energy-barrier-dependent Voc model for amorphous silicon solar cells. Appl. Phys. Lett. 109 043503 (1) - 043503 (5).

Cheyns, D., Poortmans, J., Heremans, P., Deibel, C., Verlaak, S., Rand, B.P., Genoe, J., 2008. Analytical model for the open-circuit voltage and its associated resistance in organic planar heterojunction solar cells. Phys. Rev. B 77 (16) 165332-1-10.

Choi, J.H., El-Khouly, M.E., Kim, T., Kim, Y., Yoon, U.C., Fukuzumi, S., Kim, K., 2013. Solution-processed bulk heterojunction solar cells with silyl end-capped sexithiophene. Int. J. Photoenergy 843615.

Chopra, K.L., Das, S.R., 1983. Thin Film Solar Cells. Plenum Press, New York and London, pp. 173.

Credgington, D., Durrant, J.R., 2012. Insights from transient optoelectronic analyses on the open-circuit voltage of organic solar cells. J. Phys. Chem. Lett. 3 (11), 1465–1478.

Deledalle, F., Kirchartz, T., Vezie, M.S., Campoy-Quiles, M., Tuladhar, P.S., Nelson, J., Durrant, J.R., 2015. Understanding the effect of unintentional doping on transport optimization and analysis in efficient organic bulk-heterojunction solar cells. Phys. Rev. X 5 (1) 011032-1- 011032–13.

Dibb, G., Muth, M., Kirchartz, T., Engmann, S., Hoppe, H., Gobsch, G., Thelakkat, M., Blouin, N., Tierney, S., Carrasco-Orozco, M., Durrant, J.M., Nelson, J., 2013. Influence of doping on charge carrier collection in normal and inverted geometry polymer: fullerene solar cells. Scientific Reports 3 (3335), 1–7.

Ecker, B., Nolasco, J.C., Pallarés, J., Marsal, L.F., Posdorfer, J., Parisi, J., von Hauff, E., 2011. Degradation effects related to the hole transport layer in organic solar cells. Adv. Funct. Mater. 21 (14), 2705–2711.

Fahrenbruch, A.L., Bube, R.H., 1983. Fundamentals of Solar Cells. Academic Press, USA.

Fishchuk, I.I., Kadashchuk, A., Mityashin, A., Gavrilyuk, M.M., Köhler, A., Bässler, H., Genoe, J., Sitter, H., Sariciftci, N.S., 2014. Origin of Meyer-Neldel type compensation behavior in organic semiconductors at large carrier concentrations: disorder versus thermodynamic description. Phys. Rev. B 90 (24) 245201-1- 245201–10.

Foertig, A., Rauh, J., Dyakonov, V., Deibel, C., 2012. Shockley equation parameters of P3HT:PCBM solar cells determined by transient techniques. Phys. Rev. B 86 (11) 115302–1 - 115302–7.

Garcia-Belmonte, G., 2010. Temperature dependence of open-circuit voltage in organic solar cells from generation-recombination kinetic balance. Solar Energy Mater. Solar Cells 94 (12), 2166–2169.

Gélinas, S., Rao, A., Kumar, A., Smith, S.L., Chin, A.W., Clark, J., van der Poll, T.S., Bazan, G.C., Friend, R.H., 2014. Ultrafast long-range charge separation in organic semiconductor photovoltaic diodes. Science 343 (6170), 512–516.

Goodman, A.M., 1963. Metal-semiconductor barrier height measurement by differential capacitance method-one carrier system. J. Appl. Phys. 34 (2), 329–338.

Graham, K.R., Erwin, P., Nordlund, D., Vandewal, K., Li, R., Ndjawa, G.O.N., Hoke, E., Salleo, A., Thompson, M.E., McGehee, M.D., Ammassian, A., 2013. Re-evaluating the role of sterics and electronic coupling in determining the open-circuit voltage of organic solar cells. Adv. Mater. 25 (42), 6076–6082.

Gregg, B.A., 2009. Charged defects in soft semiconductors and their influence on organic photovoltaics. Soft Matter 5 (16), 2985–2989.

Guerrero, A., Dörling, B., Ripolles-Sanchis, T., Aghamohammadi, M., Barrena, E., Campoy-Quiles, M., Garcia-Belmonte, G., 2013. Interplay between fullerene surface coverage and contact selectivity of cathode interfaces in organic solar cells. ACS Nano 7 (5), 4637–4646.

Guo, X., Zhou, N., Lou, S.J., Smith, J., Tice, D.B., Hennek, J.W., Ortiz, R.P., Lopez-Navarrete, J.T., Li, S., Strzalka, J., Chen, L.X., Chang, R.P.H., Facchetti, A., Marks, T.J., 2013. Polymer solar cells with enhanced fill factors. Nature Photon. 7 (10), 825–833.

Hallermann, M., Kriegel, I., Da Como, E., Berger, J.M., von Hauff, E., Feldmann, J., 2009. Charge transfer excitons in polymer/fullerene blends: the role of morphology and polymer chain conformation. Adv. Funct. Mater. 19 (22), 3662–3668.

Hawks, S.A., Li, G., Yang, Y., Street, R.A., 2014. Band tail recombination in polymer: fullerene organic solar cells. J. Appl. Phys. 116 (7) 074503-1-074503-11.

Hellström, S., Zhang, F., Inganäs, O., Andersson, M.R., 2009. Structure-property relationships of small bandgap conjugated polymers for solar cells. Dalton Trans. 45, 10032–10039.

Hoppe, H., Sariciftci, N.S., 2006. Morphology of polymer/fullerene bulk heterojunction solar cells. J. Mater. Chem. 16 (1), 45–61.

Hörmann, U., Kraus, J., Gruber, M., Schuhmair, C., Linderl, T., Grob, S., Kapfinger, S., Klein, K., Stutzmann, M., Krenner, H.J., Brütting, W., 2013. Quantification of energy losses in organic solar cells from temperature-dependent device characteristics. Phys. Rev. B 88 (23), 235307.

Izawa, S., Shintaku, N., Hiramoto, M., 2018. Effect of band bending and energy level alignment at the donor/acceptor interface on open-circuit voltage in organic solar cells. J. Phys. Chem. Lett. 9, 2914–2918.

Kanicki, J., 1992. Amorphous and Microcrystalline Semiconductor Devices: Materials and Device Physics. Artech house Inc., Massachusetts.

Khelifi, S., Decock, K., Lauwaert, J., Vrielinck, H., Spoltore, D., Piersimoni, F., Manca, J., Belghachi, A., Burgelman, M., 2011. Investigation of defects by admittance spectroscopy measurements in poly (3-hexylthiophene):(6,6)-phenyl C-61-butyric acid methyl ester organic solar cells degraded under air exposure. J. Appl. Phys. 110 (9) 094509-1- 094509-9.

Kim, J.Y., Kim, S.H., Lee, H., Lee, K., Ma, W., Gong, X., Heeger, A.J., 2006. New architecture for high-efficiency polymer photovoltaic cells using solution-based titanium oxide as an optical spacer. Adv. Mater. 18 (5), 572–576.

Kirchartz, T., Gong, W., Hawks, S.A., Agostinelli, T., MacKenzie, R.C.I., Yang, Y., Nelson, J., 2012. Sensitivity of the Mott-Schottky analysis in organic solar cells. J. Phys.

Chem. C 116 (14), 7672–7680.
Kirchartz, T., Deledalle, F., Tuladhar, P.S., Durrant, J.R., Nelson, J., 2013. On the differences between dark and light ideality factor in polymer: fullerene solar cells. J. Phys. Chem. Lett. 4 (14), 2371–2376.
Kniepert, J., Lange, I., van der Kaap, N.J., Koster, L.J.A., Neher, D., 2014. A conclusive view on charge generation, recombination, and extraction in as-prepared and annealed P3HT:PCBM blends: combined experimental and simulation work. Adv. Energy Mater. 4 (7) 1301401-1- 1301401–11.
Koster, L.J.A., Mihailetchi, V.D., Ramaker, R., Blom, P.W.M., 2005. Light intensity dependence of open-circuit voltage of polymer:fullerene solar cells. Appl. Phys. Lett. 86 (12) 123509–1 -123509-3.
Lange, I., Blakesley, J.C., Frisch, J., Vollmer, A., Koch, N., Neher, D., 2011. Band bending in conjugated polymer layers. Phys. Rev. Lett. 106 (21) 216402-1- 216402–4.
Li, W., Qin, R., Zhou, Y., Andersson, M., Li, F., Zhang, C., Li, B., Liu, Z., Bo, Z., Zhang, F., 2010. Tailoring side chains of low band gap polymers for high efficiency polymer solar cells. Polymer 51 (14), 3031–3038.
Lindholm, F.A., Fossum, J.G., Burgess, E.L., 1979. Application of the superposition principle to solar-cell analysis. IEEE Trans. Electron Devices 26 (3), 165–171.
Liu, A., Zhao, S., Rim, S., Wu, J., Konemann, M., Erk, P., Peumans, P., 2008. Control of electric field strength and orientation at the donor-acceptor interface in organic solar cells. Adv. Mater. 20 (5), 1065–1070.
Milnes, A.G., Feucht, D.L., 1972. Heterojunctions and Metal-Semiconductor Junctions. Academic Press, New York.
Nolasco, J.C., Sanchez-Diaz, A., Cabre, R., Ferre-Borrull, J., Marsal, L.F., Palomares, E., Pallares, J., 2010. Relation between the barrier interface and the built-in potential in pentacene/C60 solar cell. Appl. Phys. Lett. 97 (1) 013305-1-013305-3.
Nolasco, J.C., Ramos-Ortiz, G., Maldonado, J.L., Barbosa-Garcia, O., Ecker, B., von Hauff, E., 2014. Polymer/cathode interface barrier limiting the open circuit voltage in polymer: fullerene organic bulk heterojunction solar cells: a quantitative analysis. Appl. Phys. Lett. 104 (4) 043308-1- 043308–4.
Oehzelt, M., Koch, N., Heimel, G., 2014. Organic semiconductor density of states controls the energy level alignment at electrode interfaces. Nature Commun. 5 (4174), 1–8.
Perez, M.D., Borek, C., Forrest, S.R., Thompson, M.E., 2009. Molecular and morphological influences on the open circuit voltages of organic photovoltaic devices. J. Am. Chem. Soc. 131 (26), 9281–9286.
Poelking, C., Tietze, M., Elschner, C., Olthof, S., Hertel, D., Baumeier, B., Würthner, F., Meerholz, K., Leo, K., Andrienko, D., 2015. Impact of mesoscale order on open-circuit voltage in organic solar cells. Nature Mater. 14 (4), 434–439.
Potscavage, W.J., JrS, Yoo, Kippelen, B., 2008. Origin of the open-circuit voltage in multilayer heterojunction organic solar cells. Appl. Phys. Lett. 93 (19) 193308-1-193308-3.
Rau, U., Jasenek, A., Schock, H.W., Engelhardt, F., Meyer, T., 2000. Electronic loss mechanisms in chalcopyrite based heterojunction solar cells. Thin Solid Films 361, 298–302.
Rau, U., Kron, G., Werner, J.H., 2003. Reply to comments on “Electronic transport in dye-sensitized nanoporous TiO2 solar cells-comparison of electrolyte and solid-state devices. On the photovoltaic action in pn-junction and dye-sensitized solar cells. J. Phys. Chem. B 107 (48), 13547–13550.
Rauh, D., Wagenpfahl, A., Deibel, C., Dyakonov, V., 2011. Relation of open circuit voltage to charge carrier density in organic bulk heterojunction solar cells. Appl. Phys. Lett. 98 (13) 133301-1- 133301–3.
Rhoderick, E.H., 1972. Comments on the conduction mechanism in Schottky diodes. J. Phys. D-Appl. Phys. 5 (10), 1920–1929.
Riedel, I., Parisi, J., Dyakonov, V., Lutsen, L., Vanderzande, D., Hummelen, J.C., 2004. Effect of temperature and illumination on the electrical characteristics of polymer-fullerene bulk-heterojunction solar cells. Adv. Funct. Mater. 14 (1), 38–44.
Riedel, I., von Hauff, E., Parisi, J., Martin, N., Giacalone, F., Dyakonov, V., 2005. Diphenylmethanofullerenes: new and efficient acceptors in bulk-heterojunction solar cells. Adv. Funct. Mater. 15 (12), 1979–1987.
Ripolles, T.S., Guerrero, A., Garcia-Belmonte, G., 2013. Polymer defect states modulate open-circuit voltage in bulk-heterojunction solar cells. Appl. Phys. Lett. 103 (24) 243306-1-243306-5.
Schafferhans, J., Deibel, C., Dyakonov, V., 2011. Electronic trap states in methanofullerenes. Adv. Energy Mater. 1 (4), 655–660.
Scharber, M.C., Mühlbacher, D., Koppe, M., Denk, P., Waldauf, C., Heeger, A.J., Brabec, C.J, 2006. Design rules for donors in bulk-heterojunction solar cells-towards 10% energy-conversion efficiency 18, 789–79.
Schmidt, M., Korte, L., Laades, A., Stangl, R., Schubert, C., Angermann, H., Conrad, E., Maydell, K.V., 2007. Physical aspects of a-Si : H/c-Si hetero-junction solar cells. Thin Solid Films 515 (19), 7475–7480.
Shintaku, N., Hiramoto, M., Izawa, S., 2018. Doping for controlling open-circuit voltage in organic solar cells. J. Phys. Chem. C 122, 5248–5253.
Snaith, H.J., Greenham, N.C., Friend, R.H., 2004. The origin of collected charge and open-circuit voltage in blended polyfluorene photovoltaic devices. Adv. Mater. 16 (18), 1640–1645.
Steim, R., Kogler, F.R., Brabec, C.J., 2010. Interface materials for organic solar cells. J. Mater. Chem. 20 (13), 2499–2512.
Straub, A., Gebs, R., Habenicht, H., Trunk, S., Bardos, R.A., Sproul, A.B., Aberle, G., 2005. Impedance analysis: a powerful method for the determination of the doping concentration and built-in potential of non ideal semiconductor p-n diodes. J. Appl. Phys. 97 (8) 083703-1- 083703–8.
Street, R.A., Song, K.W., Cowan, S., 2011. Influence of series resistance on the photocurrent analysis of organic solar cells. Organic Electron. 12 (2), 244–248.
Sze, S.M., Ng, K.K., 1979. Physics of Semiconductor Devices, 3rd ed. John Wiley-Interscience, New York.
Tang, M.L., Okamoto, T., Bao, Z., 2006. High-performance organic semiconductors: asymmetric linear acenes containing sulphur. J. Am. Chem. Soc. 128 (50), 16002–16003.
Thompson, B.C., Frechet, J.M.J., 2008. Polymer-fullerene composite solar cells. Angew. Chem.-Int. Ed. English 47 (1), 58–77.
Tress, W., 2015. Organic Solar Cells: Theory, Experiment, and Device Simulation. Springer.
Tress, W., Leo, K., Riede, M., 2011. Influence of hole-transport layers and donor materials on open-circuit voltage and shape of I-V curves of organic solar cells. Adv. Funct. Mater. 21, 2140–2149.
Tress, W., Leo, K., Riede, M., 2013. Dominating recombination mechanisms in organic solar cells based on ZnPc and C-60. Appl. Phys. Lett. 102 (16) 163901-1- 163901–5.
Uhrich, C., Wynands, D., Olthof, S., Riede, M.K., Leo, K., Sonntag, S., Maennig, B., Pfeiffer, M., 2008. Origin of open circuit voltage in planar and bulk heterojunction organic thin-film photovoltaics depending on doped transport layers. J. Appl. Phys. 104 043107 (1) - 043107 (6).
Vandewal, K., Gadisa, A., Oosterbaan, W.D., Bertho, S., Banishoeib, F., Severen, I.V., Lutsen, L., Cleij, T.J., Vanderzande, D., Manca, J.V., 2008. The relation between open-circuit voltage and the onset of photocurrent generation by charge-transfer absorption in polymer: fullerene bulk heterojunction solar cells. Adv. Funct. Mater. 18 (14), 2064–2070.
Vandewal, K., Tvingstedt, K., Gadisa, A., Ingañäs, O., Manca, J.V., 2009. On the origin of the open-circuit voltage of polymer–fullerene solar cells. Nature Mater. 8 (11), 904–909.
Vandewal, K., Tvingstedt, K., Gadisa, A., Inganäs, O., Manca, J., 2010. Relating the open-circuit voltage to interface molecular properties of donor:acceptor bulk heterojunction solar cells. Phys. Rev. B 81 (12) 125204-1- 125204–8.
Vandewal, K., Albrecht, S., Hoke, E.T., Graham, K.R., Widmer, J., Douglas, J.D., Schubert, M., Mateker, W.R., Bloking, J.T., Burkhard, G.F., Sellinger, A., Fréchet, J.M.J., Amassian, A., Riede, M.K., McGehee, M.D., Neher, D., Salleo, A., 2014. Efficient charge generation by relaxed charge-transfer states at organic interfaces. Nature Mater. 13 (1), 63–68.
Vandewal, K., Widmer, J., Heumueller, T., Brabec, C.J., McGehee, M.D., Leo, K., Riede, M., Salleo, A., 2014. Increased open-circuit voltage of organic solar cells by reduced donor-acceptor interface area. Adv. Mater. 26 (23), 3839–3843.
Veldman, D., Ipek, Ö., Meskers, S.C.J., Sweelssen, J., Koetse, M.M., Veenstra, S.C., Kroon, J.M., van Bavel, S.S., Loos, J., Janssen, R.A.J., 2008. J. Am. Chem. Soc. 130, 7721.
von Hauff, E., Parisi, J., Dyakonov, V., 2006. Investigations of electron injection in a methanofullerene thin film transistor. J. Appl. Phys. 100 (7) 073713-1- 073713–6.
Waldauf, C., Scharber, M.C., Schilinsky, P., Hauch, J.A., Brabec, C.J., 2006. Physics of organic bulk heterojunction devices for photovoltaic applications. J. Appl. Phys. 99 (10) 104503-1-104503-6.
Wetzelaer, G.A.H., Kuik, M., Lenes, M., Blom, P.W.M., 2011. Appl. Phys. Lett. 99 (15) 153506-1- 153506–3.
Widmer, J., Tietze, M., Leo, K., Riede, M., 2013. Open-circuit voltage and effective gap of organic solar cells. Adv. Funct. Mater. 23 (46), 5814–5821.
Würfel, U., Neher, D., Spies, A., Albrecht, S., 2015. Impact of charge transport on current-voltage characteristics and power-conversion efficiency of organic solar cells. Nature Commun. 6 (6951), 1–9.
Xia, R., Leem, D., Kirchartz, T., Spencer, S., Murphy, C., He, Z., Wu, H., Su, S., Cao, Y., Kim, J.S., de Mello, J.C., Bradley, D.D.C., Nelson, J., 2013. Investigation of a conjugated polyelectrolyte interlayer for inverted polymer: fullerene solar cells. Adv. Energy Mater. 3 (6), 718–723.
Xu, Z., Chen, L., Chen, M., Li, G., Yang, Y., 2009. Energy level alignment of poly(3-hexylthiophene): [6,6]-phenyl C-61 butyric acid methyl ester bulk heterojunction. Appl. Phys. Lett. 95 (1) 013301-1- 013301–3.
Yang, B., Guo, F., Yuan, Y., Xiao, Z., Lu, Y., Dong, Q., Huang, J., 2013. Solution-processed fullerene-based organic schottky junction devices for large-open-circuit-voltage organic solar cells. Adv. Mater. 25 (4), 572–577.
Yang, B., Xiao, Z., Huang, J., 2014. Polymer aggregation correlated transition from Schottky-junction to bulk heterojunction organic solar cells. Appl. Phys. Lett. 104 (4) 143304-1- 143304–5.
Zhang, M., Wang, H., Tian, H., Geng, Y., Tang, C.W., 2011. Bulk heterojunction photovoltaic cells with low donor concentration. Adv. Mater. 23 (42), 4960–4964.